Progress In Electromagnetics Research M, Vol. 46, 173–181, 2016

Optimized Design of W-Band Quasi-Optical Lens by Using Optical Simulator and Numerical Analysis

Qike Chen*, Yong Fan, and Kaijun Song

Abstract—A large aperture quasi-optical dielectric lens antenna for passive imaging at W-band frequency is proposed. The lens is designed to obtain best resolution at a designate distance of 3.5 m from it. The lens has biconvex aspheric surface to achieve low aberration. The initial parameters of the optical path are obtained with Gaussian beam method, and then the optical simulator ZEMAX is applied to optimize the shape of the lens which improves design efficiency greatly. A hybrid numerical method is used to analyze near field distribution of the lens, and the final design of the lens is evaluated and determined by the results. The method is the combining of ANSOFT HFSS software, ray tracing method and integration algorithm based on Huygens' Principle. It is feasible and efficient for the analysis of various lens antennas, such as large aperture lens antennas which are difficult to be simulated by commercial electromagnetic simulation software. The lens is fabricated with HDPE. Experimental results show that its 3 dB beam size is 29 mm at distance of 3.5 m, which is in good agreement with theoretical calculation. The measured patterns on the image plane show that the lens has 0.3 dB decrease of field intensity in field view of 690 mm. Imaging result shows that the lens is a good candidate for focal plane imaging.

1. INTRODUCTION

Millimeter wave (MMW) can pass through non-metallic materials such as plastics or cloths with little losses and be nearly totally reflected by metallic materials. This makes MMW technology favorable for security surveillance, especially for the detection of weapons concealed under peoples' clothes [1–4]. Focal plane array (FPA) technology is useful for MMW imaging system due to its ability of greatly increasing the imaging frame rate [5].

For security surveillance, the suitable distance between target and security device is $2 \sim 4$ m. Image quality will decrease because of degradation of resolution and diffusive attenuation at such a distance for a MMW imaging system. A quasi-optical lens antenna is often used to improve these problems. The critical parameters for MMW imaging system include spatial resolution (SR), field of view (FOV) and depth of field (DOF), and all these parameters are determined by the performance of lens mostly [6]. For example, the SR depends on the beam waist radius of the lens, and the FOV is decided by the beam scanning ability of the lens. The object and image distance of lens are important issues for imaging system designed for security check too.

Previous works have demonstrated various design methods of quasi-optical lens [7–10]. Most of the lenses were designed on the basis of equivalent optical path condition and optimized by ray-tracing method. Such a method is quite suitable for lens which collimates wave into plane wave in its far-zone. However, for a quasi-optical lens which converges the incident divergent spherical wave to a point in its near zone, the method will not provide accurate results of some important parameters, such as the location and radius of beam waist of the lens, due to the effect of diffraction.

Received 8 January 2016, Accepted 23 February 2016, Scheduled 8 March 2016
* Corresponding author: Qike Chen (qkchen@uestc.edu.cn).
The authors are with the University of Electronic Science and Technology of China, China.

In this paper, a W-band quasi-optical lens antenna for focal plane MMW imaging is presented. The lens is designed to achieve beam waist radius less than 30 mm at the designate distance of 3500 mm to lens. The initial ray path parameters are calculated with Gaussian beam method, and the lens shape is optimized by optical simulator ZEMAX for low aberration. Then a hybrid numerical method is introduced to analyze the near field of the lens. HFSS software combined with aperture field integral algorithm is applied to obtain the radiation fields of the feed horns first, and then ray-tracing method is adopted for the lens part. The output field of the lens is calculated with a method based on Huygens' Principle. The numerical method is flexible and feasible for the analysis of various lenses including large aperture lens. The results of the near fields are used to evaluate the design of the lens. The lens is fabricated, and its near field patterns are measured.

2. OPTICAL PATH OF THE LENS

The quasi-optical lens is designed for a MMW imaging system with central frequency of 89 GHz. To obtain a spatial resolution of 30 mm in the object plane with a distance of 3.5 m, the lens need to form beam spots with half power beam width (HPBW) of 30 mm at that distance. 24 feed horns are packed on the focal plane to realize FOV of 690 mm in azimuth direction.

The field distributions at both sides of a lens can be described as Gaussian beams, as shown in Fig. 1. The object and image planes of the quasi-optics are positioned at beam waists where minimum beam radius occurs. According to Gaussian bean method, the HPBW of the beam spot is 2.35 times of beam radius. So we can obtain that the beam waist radius in object plane of the lens, ω_{01}, is 12.8 mm at distance of 3500 mm from lens.

For a focal plane imaging system, the value of beam waist radius on image plane, ω_{02}, is a critical parameter. A number of receivers are closely packed on the focal plane to sample the image. The spacing between receivers depends on the HPBW of the beam spot on image plane which equals $2.35\,\omega_{02}$. Small ω_{02} leads to small aperture size of the receiving antenna, and this will increase the spillover loss and reduce efficiency of the antenna. However, for large ω_{02}, the image will be poorly sampled. Therefore, the value of ω_{02} is a balanced result between efficiency and sampling rate in a practical system.

In this design, ω_{02} is chosen to be 2.6 mm, which corresponds to half power spot width of 6.1 mm. Considering that $\omega_{01} = 12.8$ mm and $S_o = 3500$ mm, $f = 592$ mm can be obtained with the following formula [11]

$$\omega_{02} = \frac{\omega_{01}}{\sqrt{(S_o/f - 1)^2 + z_c^2/f^2}} \tag{1}$$

where S_o is the distance from lens to object plane, f the focal length of the lens, and z_c the confocal distance of Gaussian beam ($z_c = \pi\omega_{01}^2/\lambda$). Then the image distance $S_i = 712$ mm can be obtained

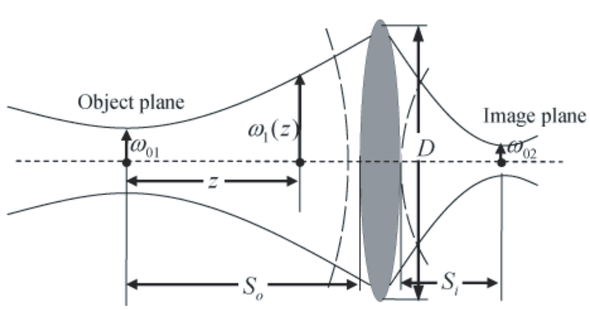

Figure 1. Sketch of Gauss beam transformation.

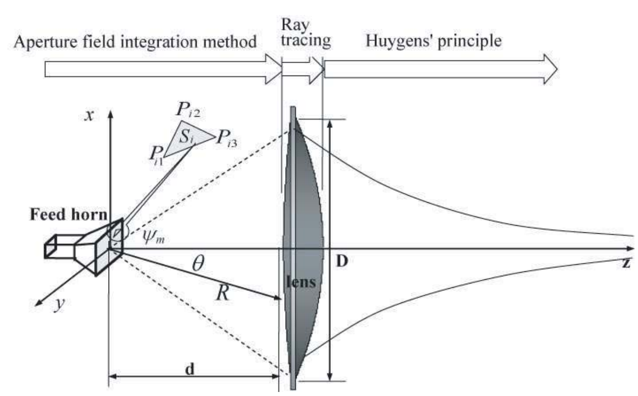

Figure 2. Quasi-optical configuration of the lens antenna.

according to Gaussian beam transformation formula:

$$S_2 = f + \frac{S_1 - f}{(S_1/f - 1)^2 + z_c^2/f^2} \tag{2}$$

The parameters of the optical path are listed in Table 1.

Table 1. Summary of optical path parameters of the lens.

Parameters	Diameters	S_o	S_i	f	Magnification (S_i/S_o)
Values	430 mm	3500 mm	712 mm	592 mm	0.203

3. QUASI-OPTICS DESIGN AND ANALYSIS

The quasi-optics configuration of the lens and feed antenna is shown in Fig. 2. The quasi-optical lens is designed with biconvex aspheric surface. Such a lens has advantage of lower aberration blurring than spherical biconvex lens and plano-convex lens. The design formula of the aspheric surface is based on the conic equation which is shown as follow:

$$z = \frac{t^2}{R + \sqrt{R^2 - (1+k)t^2}} + at^2 + bt^4 + ct^6 + dt^8 + et^{10} \tag{3}$$

where t and z are the coordinates of the lens contours; R is the curvature radius of the aspheric surface; k is the conic constant; a, b, c, d and e are the high-order coefficients of the conic equation.

The values of the coefficients in Equation (3) are optimized to achieve low aberration by optical simulator ZEMAX. It is very convenient and efficient to design MMW quasi-optical lens by using ZEMAX. However, since ZEMAX is an optical simulator designed for lights illumination system, further simulation needs to be processed to verify the design result when it is used to design MMW lens. Near field of the lens is calculated with the numeric method described in the next section, and the radius and location of the beam waist in object space are obtained to evaluate the design. Numeric result shows that the calculated S_o will be smaller than the design value in ZEMAX. For example, for lens optimized by ZEMAX with $S_o = 3500$ mm, the calculated S_o is only 3184 mm.

The final values of the constants in Equation (3) for both surfaces are given in Table 2. The diameter of the lens is 430 mm, corresponding to 128λ at central frequency 89 GHz. Material of the lens is HDPE (high density polyethylene), which has refractive index of 1.508 and loss tangent of $9 \times 10e-4$. Numeric analysis shows that S_o of the lens is 3506 mm when $S_i = 712$ mm.

As discussed in Section 1, the aperture size of the feed horn is limited to 6.1 mm. A horn with aperture size of 8.06 mm × 5.8 mm and depth of 10.4 mm was simulated and then fabricated. The horn

Table 2. Final values of the constants in Equation (3) for both surfaces of lens.

Constant	**Left**	**Right**
R	12583.41	277.78
k	2726.94	$-1.22e-2$
a	$1.17e-3$	$-2.16e-3$
b	$3.66e-10$	$-4.82e-9$
c	$-2.04e-14$	$-6.10e-14$
d	$9.26e-19$	$8.61e-19$
e	$-1.37e-23$	$-2.16e-23$

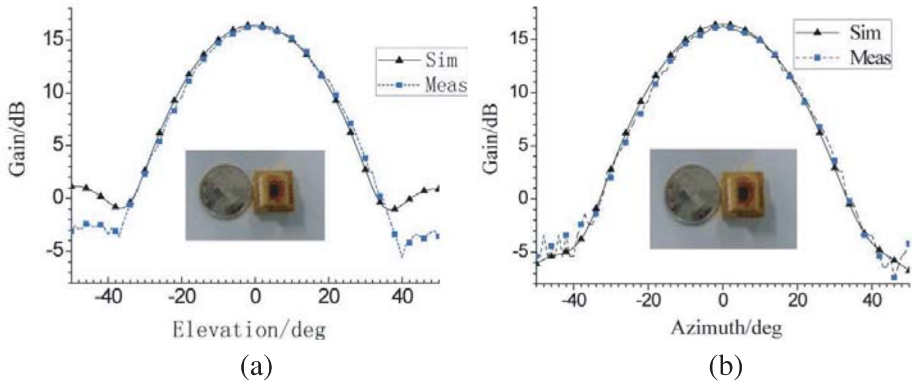

Figure 3. The simulated and measured pattern of the feed horn. (a) E-plane. (b) H-plane.

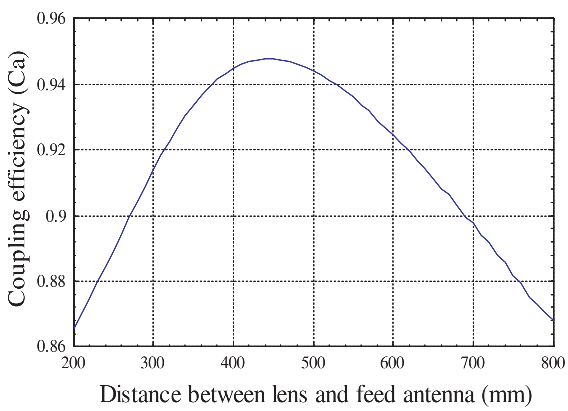

Figure 4. Field coupling efficiency c_a versus distance between lens and feed horn.

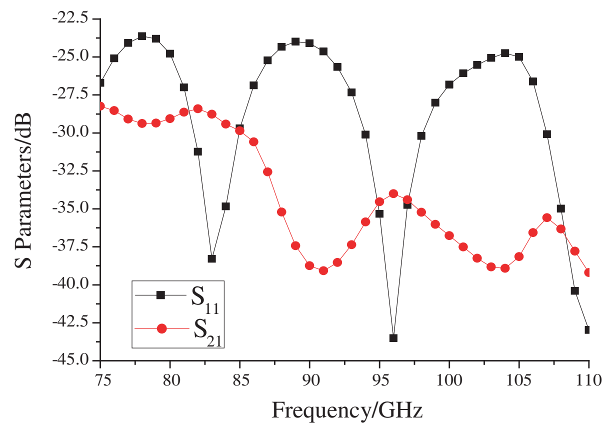

Figure 5. Simulation results of coupling between horns.

has gain about 16.2 dB, and its 10 dB beam-width at E-plane is 50° and 52° at H-plane. The simulated and measured E and H-field radiation patterns at 89 GHz frequency are depicted in Fig. 3.

The coupling efficiency between the feed horn and lens is evaluated here. The field intensity distribution of a lens is usually treated as Gaussian beam which is expressed as $q(r) \propto e^{-[r/\omega]^2}$. The transformation efficiency between Gaussian beam and the radiation pattern of the feed horn $f(\varphi)$ is depicted as follow [12]:

$$c_a = \frac{\displaystyle\int_{-\psi_m}^{\psi_m} q(r) f(\varphi) d\varphi}{\left[\displaystyle\int_{-\psi_m}^{\psi_m} |q(r)|^2 \, d\varphi \int_{-\pi/2}^{\pi/2} |f(\varphi)|^2 \, d\varphi\right]^{\frac{1}{2}}} \tag{4}$$

Since the Gaussian beam $q(r)$ is truncated at the edge of the projected aperture of the lens, the integral extends over the range which is determined by the aperture of the lens. As we can see in Fig. 2, $\psi_m = \tan^{-1}(d/2D)$, where d denotes the distance between the lens and the feed horn, which means that c_a is a function of d.

The values of c_a at various d are calculated by MATLAB and depicted in Fig. 4. $f(\varphi)$ is the E-pattern of the feed which is shown in Fig. 3. The maximum value 0.947 occurs when d equals 450 mm. When the value of d increases to 712 mm, c_a falls to 0.896. It shall be noted that the spillover loss has been included in formula (4).

The feed linear array of the lens consists of 24 horns which are closely packed on its image plane.

The mutual coupling between adjacent elements is analyzed by simulating the S parameters using ANSYS HFSS. The spacing between the horns is 6.1 mm. The simulation result is shown in Fig. 5. As we can see, S_{21} is less than -28 dB within the frequency band from 75 GHz to 110 GHz.

4. NUMERICAL ANALYSIS OF QUASI-OPTICS

To obtain the output near field of the lens, the quasi-optical configuration is divided into three parts, and three numerical methods are used to simulate the propagation of E-field within different regions, as shown in Fig. 2.

The radiation field of the feed horn is calculated with aperture field integration method. The horn aperture is meshed and split into N triangular elements by using ANSYS software first, and each triangular element has three nodes: $P_{i1}(x_{i1}, y_{i1,}z_{i1})$, $P_{i2}(x_{i2}, y_{i2,}z_{i2})$, $P_{i3}(x_{i3}, y_{i3,}z_{i3})$, as shown in Fig. 6. Then the E and H fields at all of the grid nodes are calculated with field calculator of HFSS. HFSS is a popular commercial simulator which can solve complicated electromagnetic problem with high accuracy. Then the far field of i-th triangular element can be given by [13]

$$\bar{E}_{pi} = \bar{e}_\theta E_{\theta i} + \bar{e}_\varphi E_{\varphi i} \tag{5}$$

$$\begin{aligned} E_{\theta i} &= \frac{jk}{4\pi}\frac{e^{-jkR}}{R}\left[(E_{ix}\cos\varphi + E_{iy}\sin\varphi) + \sqrt{\frac{\mu_0}{\varepsilon_0}}\cos\theta(H_{iy}\cos\varphi - H_{ix}\sin\varphi)\right]e^{jk\sin\theta(x_i\cos\varphi + y_i\sin\varphi)}S_i \\ E_\varphi &= \frac{jk}{4\pi}\frac{e^{-jkR}}{R}\left[\cos\theta(E_{iy}\cos\varphi - E_{ix}\sin\varphi) - \sqrt{\frac{\mu_0}{\varepsilon_0}}(H_{ix}\cos\varphi + H_{iy}\sin\varphi)\right]e^{jk\sin\theta(x_i\cos\varphi + y_i\sin\varphi)}S_i \end{aligned} \tag{6}$$

where x_i and y_i are the coordinates of the central point P_i of i-th element; S_i denotes the area of i-th element; R, θ, φ are the spherical coordinates of field point; E_{ix}, E_{iy}, H_{ix}, H_{iy} are the E and H field components at P_i, which can be approximated by

$$\begin{aligned} E_{ix} &= (E_{ix1} + E_{ix2} + E_{ix3})/3, \quad E_{iy} = (E_{iy1} + E_{iy2} + E_{iy3})/3 \\ H_{ix} &= (E_{ix1} + E_{ix2} + E_{ix3})/3, \quad H_{iy} = (E_{iy1} + E_{iy2} + E_{iy3})/3 \end{aligned} \tag{7}$$

By summarizing the radiation fields of all the triangular elements, the far field of the horn is obtained.

Next, ray-tracing method is processed to simulate the electromagnetic field propagating in the lens. Normally, ray-tracing method includes two steps: (1) obtaining all the ray paths based on Snell's law; (2) calculating electric fields of all rays. Considering that the circular aperture plane is the projection plane of the curved surface of the lens, we split the aperture plane into triangular elements by using ANSYS first, and the x, y coordinates of each node are given by the software. Then the value of z coordinate of each node is calculated by substituting $t = \sqrt{x^2 + y^2}$ into formula (3). Thus the curved surface at illumination side of the lens is split into triangular elements, and each node corresponds to one ray.

For single lens condition, each ray path contains two nodes located on the two surfaces of the lens. The first node P_1 is meshing grid node, and the second node P_2 is the intersection point of the refracted

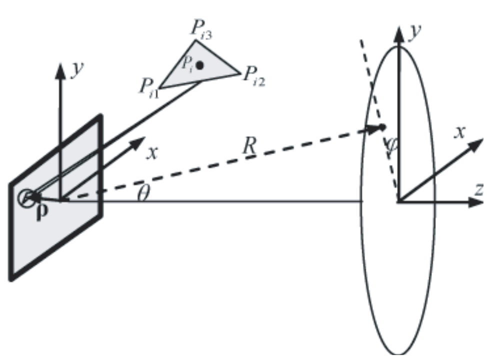

Figure 6. Geometry of the triangulation of the feed horn aperture.

ray and second surface of the lens. The coordinates of P_2 can be calculated based on Snell's law. After the ray-tracing process is completed, the second surface of the lens is split into triangular elements by the ray paths, and P_2 is taken as the grid node.

The electric fields at P_2 is calculated with method based on Fresnel's law and the law of power conservation. The incident field $\bar{E}_1^i$ at P_1 is the radiation field of the feed which is obtained with the method mentioned above. Then the incident field at P_2 is given by

$$\bar{E}_2^i = (\bar{E}_{1v}^i T_{1v} + \bar{E}_{1p}^i T_{1p}) \cdot DF_1 \cdot L_{\varepsilon_r} \cdot e^{-jkR_{12}} \tag{8}$$

where $\bar{E}_{1v}^i$ and $\bar{E}_{1p}^i$ are the components of $\bar{E}_1^i$ which are perpendicular and parallel to the incident plane respectively; T_{1v} and T_{1p} are the Fresnel transmission coefficients at P_1; R_{12} is the distance between P_1 and P_2; L_{ε_r} is the dielectric loss of the lens, which can be obtained as follow [14]

$$L_{\varepsilon_r} = 10^{-\left(\frac{27.3 \cdot R_{12}}{20\lambda} \cdot \tan\delta \cdot \frac{n}{n-1}\right)} \tag{9}$$

in which n is the index of refraction, $\tan\delta$ the loss tangent of the medium, and λ the wave length. DF_1 is the divergence factor of the ray and expressed as

$$DF_1 = \frac{1}{\sqrt{1 + R_{12}/\rho_{11}}\sqrt{1 + R_{12}/\rho_{12}}} \tag{10}$$

where (ρ_{11}, ρ_{12}) are the two principal radii of curvature of the transmitted wave front passing through point P_1, and they can be calculated by the method given by Lee et al. [15]. Finally, the refracted field $\bar{E}_2^t$ can be yielded by multiplying the transmission coefficient at P_2.

Now the seconde surface of lens is subdivided into triangular elements by the ray paths, and the field $\bar{E}_2^t$ at all the nodes is obtained. Then the output fields of lens can be calculated by the method based on Huygens' Principle, which is known as Stratton-Chu formula:

$$\bar{E}_p = -\frac{j}{4\pi\omega\varepsilon}\int_s [k^2 \bar{J}_e + (\bar{J}_e \cdot \nabla)\nabla - j\omega\varepsilon \bar{J}_m \times \nabla]\frac{\exp(-jkr_s)}{r_s} ds \tag{11}$$

Formula (11) can be expressed as follow:

$$\bar{E}_p = \bar{E}_1 + \bar{E}_2 + \bar{E}_3 \tag{12}$$

in which

$$\begin{aligned}
\bar{E}_1 &= -\frac{jk^2}{4\pi\omega\varepsilon}\sum_{i=1}^{N}\left[-(\bar{J}_{ei} \cdot \bar{r}_{si})\bar{r}_{si} + \bar{J}_{ei} + \sqrt{\frac{\varepsilon}{\mu}}\bar{J}_{mi} \times \bar{r}_{si}\right]\frac{\exp(-jkr_{si})}{r_{si}}\Delta s_i \\
\bar{E}_2 &= -\frac{j^2 k}{4\pi\omega\varepsilon}\sum_{i=1}^{N}\left[3(\bar{J}_{ei} \cdot \bar{r}_{si})\bar{r}_{si} - \bar{J}_{ei} - \sqrt{\frac{\varepsilon}{\mu}}\bar{J}_{mi} \times \bar{r}_{si}\right]\frac{\exp(-jkr_{si})}{r_{si}^2}\Delta s_i \\
\bar{E}_3 &= -\frac{j}{4\pi\omega\varepsilon}\sum_{i=1}^{N}[3(\bar{J}_{ei} \cdot \bar{r}_{si})\bar{r}_{si} - \bar{J}_{ei}]\frac{\exp(-jkr_{si})}{r_{si}^3}\Delta s_i
\end{aligned} \tag{13}$$

where N is the number of the grid elements; $\bar{r}_{si}$ is the unit vector in the direction from i-th element to field point; Δs_i is the area of the i-th triangular element; $\bar{J}_{ei}$ and $\bar{J}_{mi}$ are the equivalent current and magnetic current at i-th triangular element, which are

$$\bar{J}_{ei} = \bar{n}_i \times \bar{H}_{si}, \quad \bar{J}_{mi} = -\bar{n}_i \times \bar{E}_{si} \tag{14}$$

in which $\bar{n}_i$ is the unit normal vector of i-th triangle, and $\bar{E}_{si}$ and $\bar{H}_{si}$ are the average fields of the three nodes of i-th triangular element.

The electric field distribution on the optical axis and the beam pattern at the waist of the lens were calculated with the hybrid numerical method. To evaluate the effectiveness of the method, we simulated the near field of the lens using FEKO 5.5, and then both of the results were compared with the measurement results. The results of electric field distribution on the optical axis are shown in Fig. 7. It can be seen that the numerical results are closer to the measurement results than FEKO's. The maximum power occurs at 3460 mm in numerical method, which is close to the measured value of

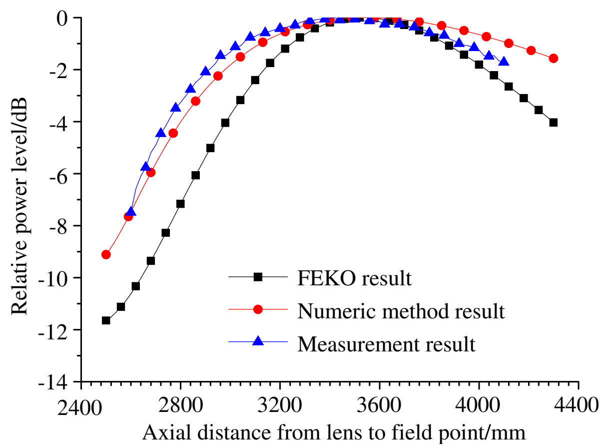

Figure 7. Numerical and measurement result of electric field distribution along optical axis comparing with FEKO simulation result.

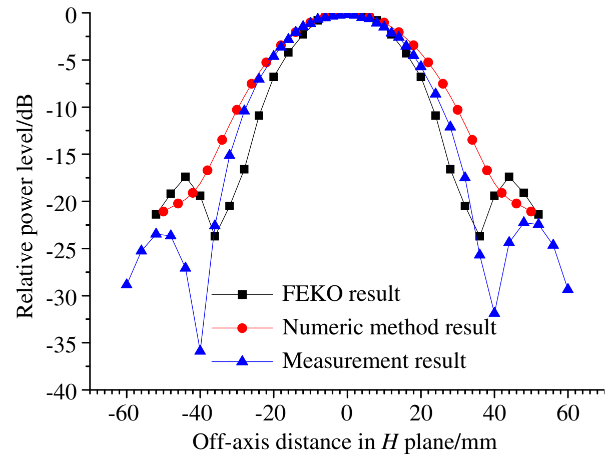

Figure 8. Theoretical and measurement result of H-plane pattern at the beam waist of the lens.

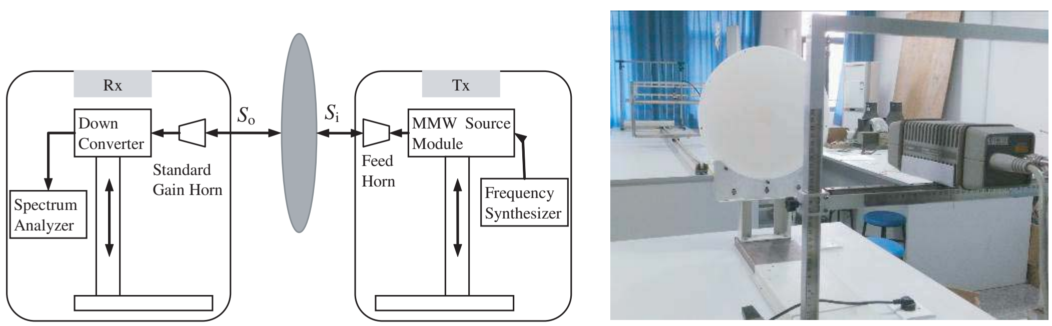

(a) (b)

Figure 9. (a) Block diagram and (b) photograph of the measurement setup.

3420 mm. The H-plane pattern at beam waist of the lens is also calculated with numeric method and FEKO, and the results are shown in Fig. 8. The HPBW of the pattern of the numeric result is about 33 mm, which is slightly broader than the measurement result of 29.5 mm.

The hybrid numerical method is very flexible and suitable for analyzing various lenses. Moreover, the method has an advantage in computational time. For the lens proposed in this paper, it takes only about 2.5 seconds to calculate the field at one field point, versus 13 seconds with the FEKO software on the same computer which has processor of core i5 with a CPU frequency of 2.6 GHz and 4 GB of RAM.

5. EXPERIMENT RESULT

The quasi-optical lens antenna was fabricated and measured. The quasi-optics experiment setup is shown in Fig. 9. The transmitter was composed of a feed horn and a W-band source generator. A standard gain horn connected with a harmonic down-conversion mixer was applied as receiver, and a spectrum analyzer was used to measure and display the received power. The receiver was placed in object space, and the transmitter was placed in image space. To measure the near-field pattern of the lens, both the transmitter and receiver were fixed on mechanisms which could move in x, y, z directions.

The focal length f was tested first. The distance between the receiver and the lens was fixed at 3500 mm, and then the transmitter was scanned on the optical axis of lens. The focal point was obtained when the maximum power was observed. As we can see in Fig. 10, the maximum power occurs at $S_i = 682$ mm. According to the thin lens equation, the actual value of focal length f of the lens is

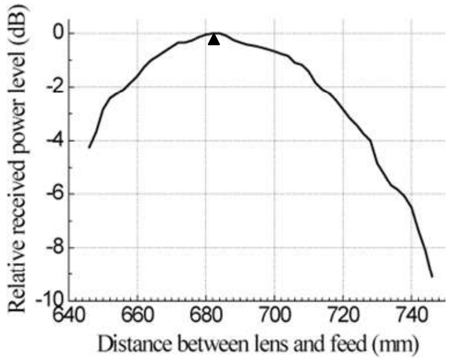

Figure 10. Relative received power at various image distance ($S_o = 3500\,\mathrm{mm}$).

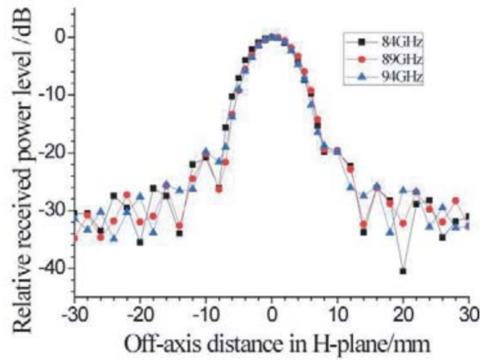

Figure 11. H-plane beam pattern of the lens at various frequency ($S_i = 682\,\mathrm{mm}$, $S_o = 3500\,\mathrm{mm}$).

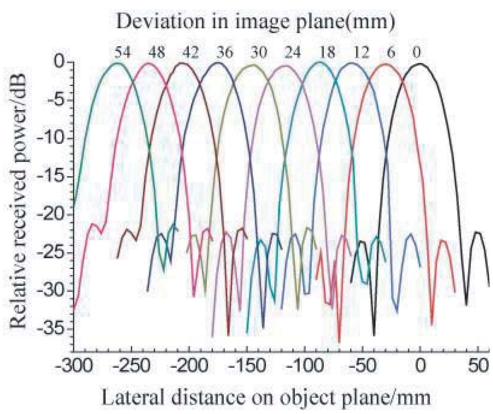

Figure 12. Measured beam patterns on the object plane.

(a) (b)

Figure 13. (a) Photos of the PMMW imaging system and (b) the imaging result of concealed objects under clothes.

about 571 mm, which is 21 mm smaller than the theoretical value. The difference between the measured value and theoretical value of focal length can be caused by the difference between actual and theoretical value of the dielectric constant of HDPE at W-band.

Then the transmitter and receiver were positioned at $S_i = 682\,\mathrm{mm}$ and $S_o = 3500\,\mathrm{mm}$, respectively. The beam patterns in the image plane at 84, 89, 94 GHz frequency were measured by scanning the transmitter laterally. Measurement results show that the beam patterns are similar for all frequencies, and the 3 dB beam size in the image plane is about 6.4 mm (as seen in Fig. 11).

Further, the measurement of the beam patterns for different lateral deviations were performed. Fig. 12 shows the measured beam patterns on the object plane. The patterns correspond to the situation that the transmitter deviates the optical axis laterally 0 mm, 6 mm, 12 mm, ..., 54 mm in the image plane respectively. As we can see, the HPBW of the beam spot is about 29 mm, and the power intensity fluctuation is less than 0.3 dB.

The quasi-optical lens was applied to the PMMW imaging system. The optical subsystem of the imaging system was composed of the dielectric lens, a 24-channel sensor array and a flapping reflector, as shown in Fig. 13. The imaging sensor array was arranged in a line and located at focal plane of the lens to obtain a field of view of 690 mm × 1800 mm. The speed of the flapping reflector was regulated so as to realize a frame rate of 4 Hz. Imaging of concealed objects in clothes was performed in the laboratory. A thin metal in the shape of pistol was concealed under clothes of the experimenter, and a hand phone was put in his right trouser pocket. As we can see in Fig. 13, clear images of both targets are obtained in the original MMW image, and the shapes of the targets are shown correctly. Moreover, the image of belt buckle is also displayed.

6. CONCLUSION

A large aperture quasi-optical lens antenna used for W-band focal plane millimeter wave imaging has been developed. The shape of the lens was optimized with commercial optical simulator ZEMAX. A flexible and efficient hybrid numerical method was introduced to optimize the design so as to obtain best spatial resolution at designate object distance. Prototype of the lens was fabricated and measured. The lens has an effective focal length of 571 mm and 3 dB beam size about 30 mm on object plane. Experimental results agrees with the numerical calculation quite well.

REFERENCES

1. Yujiri, L., M. Shoucri, and P. Moffa, "Passive millimeter wave imaging," *IEEE Microwave Magazine*, Vol. 4, No. 3, 39–50, 2003.
2. Stanko, S., D. Notel, A. Wahlen, et al., "Active and passive mm-wave imaging for concealed weapon detection and surveillance," *The 33rd International Conference on Infrared, Millimeter and Terahertz Waves*, 1–2, 2008.
3. Pati, P. and P. Mather, "Open area concealed weapon detection system," *Proceeding of SPIE 8017, Detection and Sensing of Mines, Explosive Objects, and Obscured Targets XVI*, 801702-1–801702-9, Orlando, 2011.
4. Shi, X. and M. H. Yang, "Development of passive millimeter wave imaging for concealed weapon detection indoors," *Microwave and Optical Technology Letters*, Vol. 56, No. 7, 1701–1706, 2014.
5. Sato, S, K. Sawaya, K. Mizuno, et al., "Passive millimeter-wave imaging for security and safety applications," *Proceedings of SPIE 7671, Terahertz Physics, Devices, and Systems*, 76710V-1–76710V-11, 2010.
6. Kim, W. G., N. W. Moon, M. K. Singh, et al., "Characteristic analysis of aspheric quasi optical lens antenna in millimeter-wave radiometer imaging system," *Applied Optics*, Vol. 52, No. 6, 1122–1131, 2013.
7. Thakur, J. P., W.-G. Kim, and Y.-H. Kim, "Large aperture low aberration aspheric dielectric lens antenna for W-band quasi optics," *Progress In Electromagnetics Research*, Vol. 103, 57–65, 2010.
8. Qiu, J., Z. Zhuang, X. Han, and F. Xie, "Design of quasi-optical subsystem for millimeter-wave imaging system," *International Symposium on Antennas Propagation & Em Theory*, 530–533, 2008.
9. Volkov, P. V., Yu. I. Belov, A. V. Goryunov, I. A. Illarionov, et al., "Aspherical single-lens objective for radio-vision systems of the millimeter-wavelength range," *Technical Physics*, Vol. 59, No. 4, 588–593, 2014.
10. Richter, J., A. Hofmann, and L. P. Schmidt, "Dielectric wide angle lenses for millimeter-wave focal plane imaging," *European Microwave Conference*, 1–4, 2001.
11. Goldsmith, P. F., "Quasi-optical techniques," *Proceedings of the IEEE*, Vol. 80, No. 11, 1729–1747, 1992.
12. Goldsmith, P. F., *Quasi Optical Systems: Gaussian Beam Quasi Optical Propagation and Applications*, 130–133, IEEE Press/Chapman & Hall Publishers, Piscataway, 1998.
13. Zhang, Y., J. Wang, Z. Zhao, and J. Yang, "Numerical analysis of dielectric lens antennas using a ray-tracing method and HFSS software," *IEEE Antennas & Propagation Magazine*, Vol. 50, No. 4, 94–101, 2008.
14. Kim, W.-G., N.-W. Moon, J. Kang, and Y.-H. Kim, "Loss Measuring of large aperture quasi-optics for W-band imaging radiometer system," *Progress In Electromagnetics Research*, Vol. 125, 295–309, 2012.
15. Lee, S.-W., M. S. Sheshadri, V. Jamnejad, and R. Mittra, "Refraction at a curved dielectric interface: geometrical optics solution," *IEEE Transactions on Microwave Theory and Techniques*, Vol. 82, No. 1, 12–19, 1982.